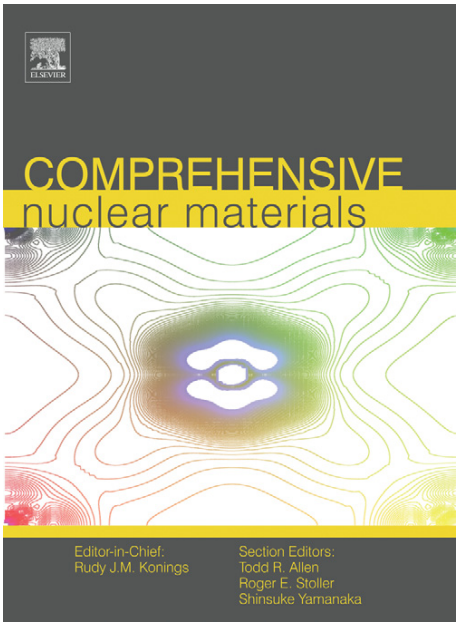

Allen T.R., Konings R.J.M., and Motta A.T. (2012) Corrosion of Zirconium Alloys. In: Konings R.J.M., (ed.) Comprehensive Nuclear Materials, volume 5, pp. 49-68 Amsterdam: Elsevier.

5.03 Corrosion of Zirconium Alloys

T. R. Allen
University of Wisconsin, Madison, WI, USA
R. J. M. Konings
European Commission, Joint Research Centre, Institute for Transuranium Elements, Karlsruhe, Germany
A. T. Motta
The Pennsylvania State University, University Park, PA, USA

Abbreviations

BWR	Boiling water reactor
CANDU	Canadian Deuterium Uranium
CRUD	Chalk River unidentified deposits
DHC	Delayed hydride cracking
IAEA	International Atomic Energy Agency
M5™	Zirconium alloy material with niobium (AREVA)
PWR	Pressurized water reactor
tHM	Ton heavy metal
VVER	Voda Voda Energy Reactor
ZIRLO™	Zirconium alloy material with niobium, tin, and iron (Westinghouse)
Zry	Zircaloy

5.03.1 Introduction

Zirconium alloys are widely used for fuel cladding and in pressure tubes, fuel channels (boxes), and fuel spacer grids in almost all water-cooled reactors: light water reactors such as the pressurized water reactor (PWR) and the boiling water reactor (BWR) as well as the Canadian designed Canadian Deuterium Uranium (CANDU) heavy water reactor. Since its employment in the first commercial nuclear power plant (Shippingport) in the 1960s, Zircaloy, a zirconium–tin alloy, has shown satisfactory behavior during many decades. However, degradation due to waterside corrosion can limit the in-reactor design life of the nuclear fuel. The critical phenomenon is the

Comprehensive Nuclear Materials (2012), vol. 5, pp. 49-68

hydrogen ingress into the cladding during corrosion, which can cause cladding embrittlement. As utilities are striving to achieve higher fuel burnups, the nuclear industry has made several efforts to understand the mechanisms of corrosion and to mitigate its effects.

In striving for increased burnup of the nuclear fuel from 33 000 to 50 000 MWd/tHM and beyond in PWRs, associated studies have shown that the corrosion of the Zircaloy-4 cladding accelerates under these higher burnup conditions. Although alloys that are more modern have not yet shown evidence of this high-burnup acceleration, this is a potential concern. Also, the efforts to increase the thermal-cycle efficiency in PWRs by operating at higher temperatures (power uprates), combined with the more aggressive chemistry (introduction of B and Li for example) related to the use of high-burnup fuel, have resulted in increased fuel duty,[1] and in increased corrosion rates. This has led to the introduction of cladding tubes of new zirconium alloys such as zirconium–niobium, which are much more corrosion resistant.[2,3] With the introduction of these materials, the nuclear industry aims at zero tolerance for fuel failure in the future.[4]

Many reviews on the corrosion of zirconium alloys both out- and in-reactor, have been published.[5–11] The extensive reviews made by an international expert group of the International Atomic Energy Agency (IAEA) and published as IAEA-TECDOCs 684 and 996[12,13] are major references in this respect. As mentioned by Cox,[6,7] "the number of publications on this topic is so enormous that it is impossible for a short review to be comprehensive." This also applies to the current chapter, which therefore focuses on the main issues, naturally relying on the above-mentioned existing reviews and updating the information where possible with new results and insights.

5.03.2 General Considerations

5.03.2.1 Oxidation

Corrosion of zirconium alloys in an aqueous environment is principally related to the oxidation of the zirconium by the oxygen in the coolant, dissolved or produced by radiolysis of water. A small amount of oxygen can be dissolved in the metal, but once the thermodynamic solubility limit is exceeded, ZrO_2 is formed on the metal. (All zirconium components normally have a thin oxide film (2–5 nm) on their surface in their as-fabricated state.) The oxide formed is protective, thus limiting the access of oxidizing species to the bare metal. Much evidence exists to indicate that Zr oxidation occurs by inward migration of oxygen ions through the oxide layer, either through grain boundaries or through the bulk.[5,12,13]

$$Zr + O_2 = ZrO_2$$

As shown in **Figure 1**, the growth of the oxide layer on the metal surface depends on the kinetics of the oxygen diffusion through this layer. Because the corrosion kinetics slow down as the oxide thickness increases, it has been argued that the rate controlling step in the oxidation process is the transport of atomic species in the protective oxide, by either oxygen diffusion through the oxide film[14,15] or diffusion of electrons through the oxide film. These processes are necessarily coupled to maintain electroneutrality. Electron transport is, however, difficult in zirconium dioxide, as it is an electrical insulator when undoped. Although this is not positively confirmed, it is likely that the role of doping elements in the determination of corrosion kinetics is done through their influence on the electron or oxygen transport in the oxide layer.

Several types of corrosion morphologies have been observed in nuclear reactors and in autoclave experiments, of which the most important are

1. *Uniform*: The formation of a thin uniform layer of zirconium dioxide on the surface of a zirconium alloy component (see **Figure 2**).
2. *Nodular*: The formation of local, small, circular zirconium oxide blisters (see **Figure 3**).
3. *Shadow*: The formation of local corrosion regions that mirror the shape (suggestive of a shadow) of other nearby noble reactor core components (**Figure 4**).

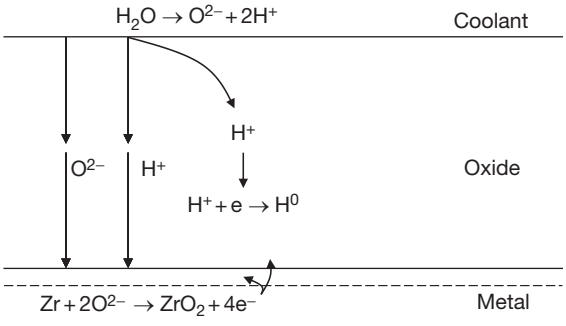

Figure 1 Schematic presentation of the corrosion of the zirconium alloys. Corrosion of zirconium alloys in nuclear power plants; TECDOC-684; International Atomic Energy Agency, Vienna, Austria, Jan 1993.

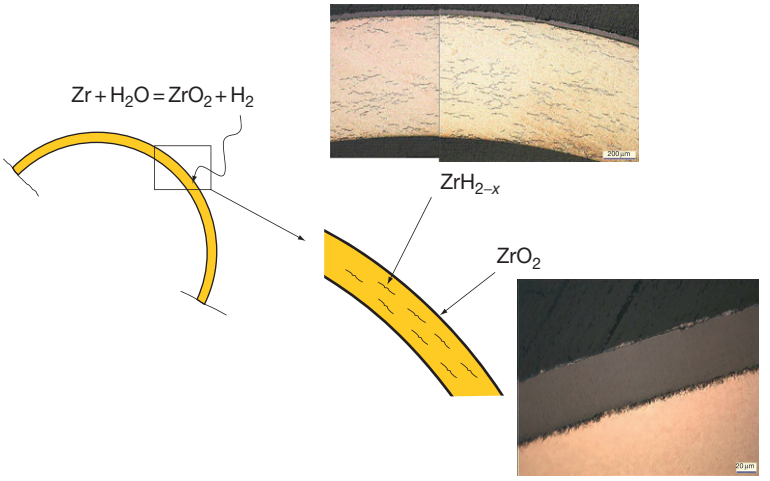

Figure 2 Uniform oxide layer formation and hydride precipitation in Zircaloy cladding. © European Atomic Energy Commission.

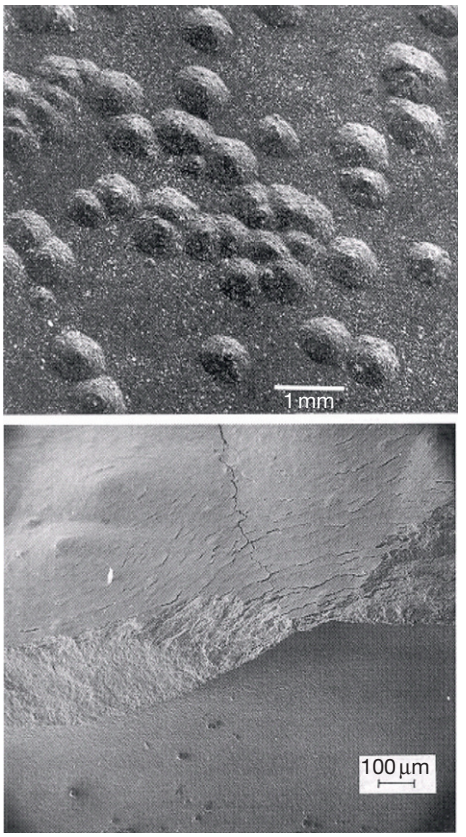

Figure 3 General appearance of nodules formed on zirconium alloy following a 500 °C steam test at 10.3 MPa. In the bottom, a cross-section view of a nodule is shown, exhibiting circumferential and vertical cracks. Photo courtesy of R. Ploc and NFIR (Nuclear Fuel Industry Research Group). Reproduced from Lemaignan, C.; Motta, A. T. Zirconium Alloys in Nuclear Applications, Materials Science and Technology, Nuclear Materials Pt. 2; VCH Verlagsgesellschaft mbH, Weinheim, Germany, 1994.

The occurrence of these morphologies is strongly dependent on the reactor operating conditions and chemical environment (particularly the concentration of oxygen in the coolant), which are distinctly different in PWRs, BWRs, and CANDU (**Table 1**). In both BWRs and PWRs, a uniform oxide layer is observed, although its thickness is normally greater in PWR than in BWR, primarily because of the higher operating temperature. Nodular corrosion occurs occasionally in BWRs because a much higher oxygen concentration occurs in the coolant because of water radiolysis and boiling. Shadow corrosion is also occasionally observed in BWRs and is a form of galvanic corrosion.

5.03.2.2 Hydrogen Uptake

The formation of an oxide layer would not bring severe consequences to cladding behavior were it not for the fact that in parallel with the corrosion process, a fraction of the hydrogen, primarily produced by the oxidation reaction as well as by radiolysis of water, diffuses through the oxide layer into the metal. Zirconium has a very low solubility for hydrogen (about 80 wt ppm at 300 °C and 200 wt ppm at 400 °C) and once the solubility limit is exceeded, the hydrogen precipitates as a zirconium hydride phase (**Figure 2**):

$$\mathrm{Zr(H,sln) + H_2 = ZrH_{1.6}\ or\ ZrH_2}$$

As a result, the following effects have been reported (although not all confirmed) to occur in the cladding: hydrogen embrittlement due to excess hydrogen or its localization into a blister or rim,[16,17] loss of

fracture toughness, delayed hydride cracking (DHC), and acceleration of corrosion and of irradiation growth. Hydrogen embrittlement impacts the mechanical resistance of the Zircaloy cladding to failure and it is thus of key importance to understand its underlying mechanisms. The ductility reduction due to hydrogen embrittlement is dependent on the volume fraction of hydride present, the orientation of the hydride precipitates in the cladding, and their degree of agglomeration.[18,19]

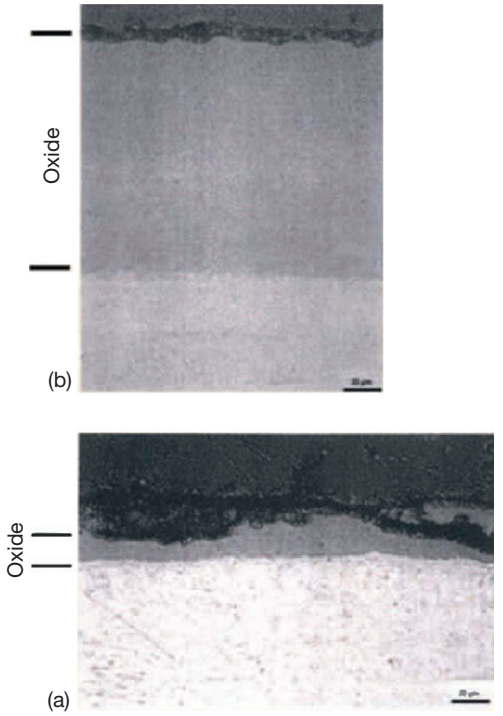

Figure 4 Zirconium oxides near (b) and away from (a) a stainless steel control blade bundle, showing the effect of shadow corrosion. Reproduced from Adamson, R. B.; Lutz, D. R.; Davies, J. H. Hot cell observations of shadow corrosion phenomena. In *Proceedings Fachtagung der KTG-Fachgruppe, Brennelemente und Kernbautelle*, Forschungszentrum Karlsruhe, Feb 29–Mar 1, 2000.

5.03.2.3 Controlling Factors for Corrosion

The oxidation and hydrogen uptake of Zircaloy is of course determined by many factors. First of all, the chemical and physical state of the material: composition, metallurgical condition, and surface condition. These conditions are often specific to the material and sometimes batch-specific and also related to the fabrication process, as discussed in detail in **Chapter 2.07, Zirconium Alloys: Properties and Characteristics**. This is evident from the different behavior of Zircaloy and Zr–Nb alloys, as shown in **Figure 5** for two different zirconium alloys employed in the French PWRs, Zircaloy and Zr1% Nb (M5). The peak oxide layer thickness of Zircaloy-4 (oxide thickness at the hottest fuel grid span) increases significantly with burnup (i.e., residence time in the reactor), whereas that of Zr1%Nb shows a moderate increase.

In addition, a number of environmental factors affecting the corrosion of zirconium alloys must be considered:

1. *Coolant Chemistry*: It is obvious that the dissolved oxygen and hydrogen play a major role in the corrosion process, but other dissolved species must also be taken into account. To control the pH of the coolant at slightly alkaline conditions,

Table 1 Typical reactor environments to which the zirconium alloys are exposed

	BWR	*PWR*	*VVER*	*CANDU*
Coolant	H_2O	H_2O	H_2O	D_2O
Inlet temperature (°C)	272–278	280–295	290	255
Outlet temperature (°C)	280–300	310–330	320	300
Pressure (MPa)	~7	~15	~15	~10
Neutron flux[a] ($n\,cm^{-2}\,s^{-1}$)	$4–7 \times 10^{13}$	$6–9 \times 10^{13}$	$5–7 \times 10^{13}$	2×10^{12}
Coolant chemistry				
$[O_2]$ (ppb)	~200	<0.05	< 0.1	<5
$[H_2]$ (ppm)	~0.03	2–5	–	0.5–1
pH	7	6.9–7.4		10.2–10.8
B (as H_3BO_3) (ppm)	–	0–2200	0–1400[16]	–
Li (as LiOH) (ppm)	–	0.5–5	0.05–0.6	1
Na (as NaOH) (ppm)	–	–	0.03–0.35	–
K (as KOH) (ppm)	–	–	5–20	–
NH_3 (ppm)	–	–	6–30	–

[a] $E > 1$ MeV.
Corrosion of zirconium alloys in nuclear power plants; TECDOC-684; International Atomic Energy Agency, Vienna, Austria, Jan 1993.

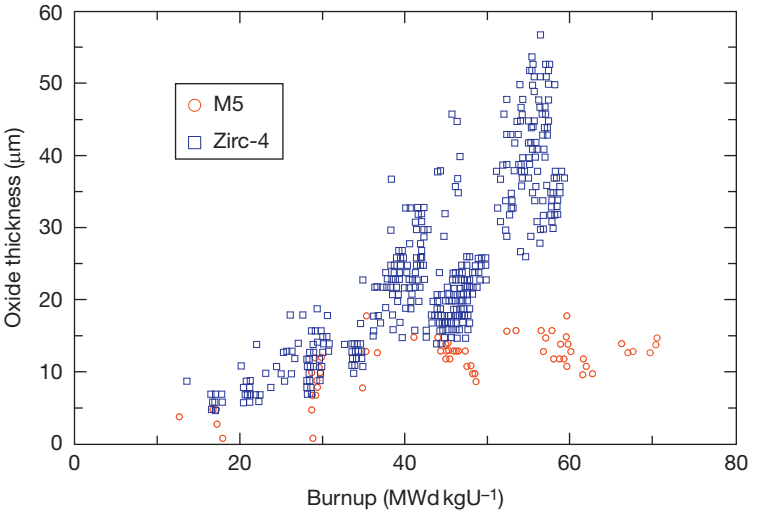

Figure 5 Peak oxide layer thickness as a function of burnup for Zircaloy-4 and Zr1%Nb (M5). Reproduced from Bossis, P.; Pêcheur, D.; Hanifi, K.; Thomazet, J.; Blat, M. *J. ASTM Int.* **2006**, *3*(1), Paper ID JAI12404.

LiOH is added and H_3BO_3 (boric acid) is added for reactivity control in PWRs. Furthermore, impurities (Cl, F) and coolant-borne species (Cu, Ni, etc.) must be considered.

2. *Radiation*: In reactor, the Zircaloy and the coolant are subjected to the effects of energetic particles. The principal effect is the production of oxidizing species such as O_2 in the coolant.
3. *Temperature*: In the range of water reactor operation (~240–330 °C), the combined effect of temperature and radiation on zirconium alloy oxidation and hydriding have been characterized extensively, varying from almost no effect to acceleration of oxidation by factors of up to two orders of magnitude, depending on environment and radiation level.
4. In addition, the presence of boiling and CRUD (the term CRUD stands for Chalk River unidentified deposits, the nuclear power plant in which the effect was observed for the first time) deposition in PWR can enhance corrosion.

5.03.3 Uniform Oxidation

5.03.3.1 Mechanism

Uniform corrosion is defined as a process that occurs approximately with the same speed on the entire surface of an object (ISO 8044). It can be considered as an electrochemical cell process, in which the metal is anodically oxidized:

$$Zr + 2O^{2-} = ZrO_2 + 2V_O^{o} + 4e^{-}$$

where V_O^{o} indicates a lattice vacancy in the ZrO_2 layer. The corresponding cathodic reaction at the oxide/coolant interface can be the reduction of water:

$$2H_2O + 4e^{-} + 2V_O^{o} = 2O^{2-} + 4H^{\cdot}$$

or, when the water contains dissolved oxygen:

$$2H_2O + O_2 + 2V_O^{o} + 4e^{-} = 4OH^{\cdot}$$

The oxygen ions diffuse preferentially via the oxide crystallite boundaries to the oxide/metal interface, whereas the vacancies diffuse in the opposite direction. The hydrogen can combine with electrons to form atomic/molecular hydrogen that dissolves in the coolant water or diffuses to the metal.

Uniform corrosion is a passivating event since a protective layer of zirconium oxide is formed as a result of the reaction with the O^{2-} ions or the $OH^{\cdot}$ radicals. Electron microscopy shows that the oxide layer is microcrystalline, initially equiaxed, later growing into columnar grains that are formed in a dense packing, of which the mean crystallite size increases as the oxide thickens.[15] **Figure 6** shows typical microstructures of the oxide layer for several zirconium-based cladding materials. **Figure 6(c)**, in particular, shows the columnar grains extending right near the oxide/metal interface.

The corrosion kinetics have been studied extensively. As mentioned above, because the corrosion rate slows down with oxide thickness, the rate controlling step is thought to be the transport of oxidizing species in the layer.[15,20] During corrosion,

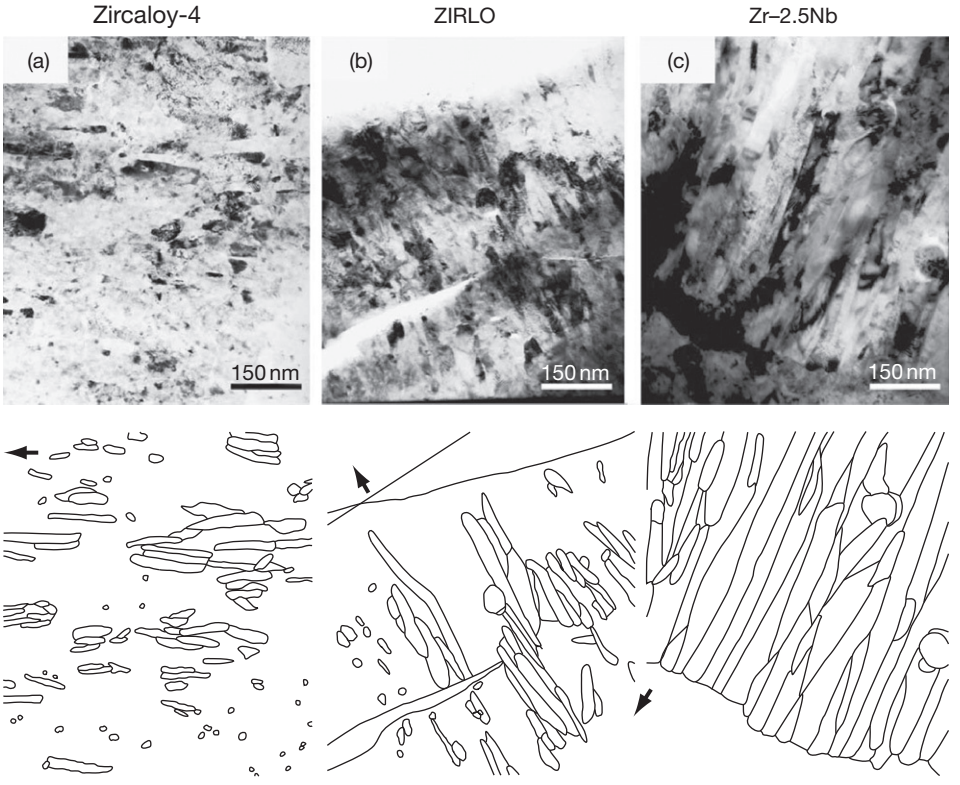

Figure 6 Grain size, shape, and orientation comparison near the oxide/metal interface of (a) Zircaloy-4, (b) ZIRLO, and (c) Zr–2.5Nb alloy oxides formed in 360 °C pure water environments. The hand-drawn sketch below each bright-field image shows oxide crystallite grain boundaries. Black arrows indicate oxide growth direction. Reproduced from Yilmazbayhan, A.; Breval, E.; Motta, A. T.; Comstock, R. J. *J. Nucl. Mater*. **2006**, *349*, 265–281.

a potential develops across the oxide layer. The negative potential at the oxide/metal interface accelerates the electron migration process and retards the O^{2-} diffusion until both operate at the same rate. Bossis *et al.*[22] argue that the surface reactions are rate-determining in some Nb-containing alloys.

The measurements of the weight gain kinetics for zirconium and its alloys (the weight gain is due to oxygen ingress and follows the overall corrosion kinetics) were found to fall into two stages, referred to as pre- and posttransition. For constant temperature and pressure, the pretransition corrosion kinetics are independent of pH between about 1 and 13 (if no specifically aggressive species such as LiOH are present) and of the source of the oxygen. The kinetics of the pretransition oxide layer formation, as measured from weight gain (ΔW), have been found to approximately follow a cubic rate law[21]:

$$(\Delta W)^3 = k_1 t \qquad [1]$$

where k_1 is the preexponential factor and t is time. More recent results have shown that the rate law depends on the alloys according to $(\Delta W)^n = kt$, with n between 2 and 5.[22] The temperature dependence of k_1 follows an Arrhenius-type equation:

$$k_1 = B_1 \exp\left(\frac{-Q_1}{RT}\right) \qquad [2]$$

where B_1 is an empirical constant, R is the universal gas constant, T is the absolute temperature, and Q_1 is the activation energy for pretransition oxidation. The values for B_1 are Q_1 are obtained empirically from fitting of experimental data, for example, $B_1 = 6.36 \times 10^{11}\,(\text{mg dm}^{-2})^3$ per day and $Q_1/R = 13640$ K, as found by Kass[21] for Zry-2 and Zry-4.

The posttransition kinetics, on the contrary, are approximately linear ($n = 1$) in time[23]:

$$\Delta W = k_2 t + C \qquad [3]$$

with

$$k_2 = B_2 \exp\left(\frac{-Q_2}{RT}\right) \qquad [4]$$

and C the weight gain at transition. B_2 is the empirical constant and Q_2 the activation energy for posttransition

oxidation. Hillner *et al.*[23] discussed the results of numerous analyses of experimental corrosion studies on Zircaloy with varying time and temperature to derive B_2 and Q_2. As discussed by these authors, most studies suffer from paucity of data for extended exposures. Their own results for Zry-2 and Zry-4 cover a wide range of time and weight gain and the posttransition kinetics were interpreted to consist of two linear stages (with a change at about 400 mg dm^{-2} or about 30 μm) with $B_2 = 2.47 \times 10^8$ mg dm^{-2} day^{-1} and $Q_2/R = 12880$ K for stage 1, and $B_2 = 3.47 \times 10^7$ mg dm^{-2}day^{-1} and $Q_2/R = 11452$ K for stage 2. Whether or not Hillner's interpretation of a change in mechanism is correct, certainly the data is best described by a two-stage empirical fit.

A schematic representation of these pre- and posttransition kinetics is shown in **Figure 7** as the dashed lines. Also shown in this graph is the more recent view that three stages can be discriminated for zirconium alloy corrosion processes[23]:

1. The early pretransition regime, characterized by the formation of a thin, black, tightly adherent corrosion film that grows thicker in accordance with a nearly cubic rate law.
2. The intermediate stage that lies between the pre- and posttransition stages. As initially shown by Bryner,[24] this region appears to comprise a series of successive cubic curves, similar to the initial cubic kinetic curve. This linear rate results from the superposition of various regions of the oxide layer following pretransition growth rate but slightly out of phase with each other.
3. The linear posttransition kinetic regime.

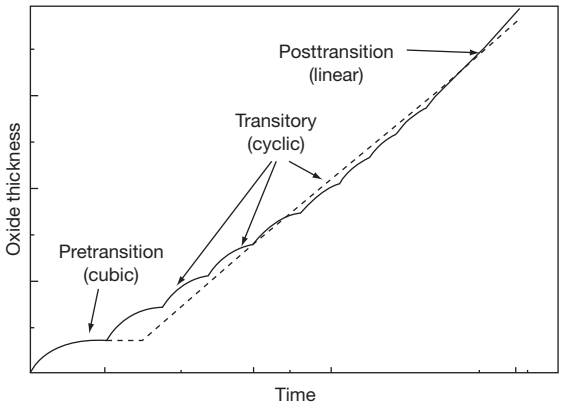

Figure 7 Schematic representation of the zirconium alloy corrosion showing the pretransition, transitory, and posttransition regions. The dashed lines indicate early models that recognized only the pre- and posttransition regimes. Reproduced from Hillner, E.; Franklin, D. G.; Smee, J. D. *J. Nucl. Mater.* **2000**, *278*, 334.

In the very early stages of the oxide formation, the layer is dense and composed of grains that have a predominantly tetragonal or cubic structure. As the grains grow, columnar grain growth is established and the tetragonal grains tend to transform to monoclinic oxide, which constitutes the majority of the oxide formed.[20] Although the tetragonal phase has often been associated with protective behavior, this correlation is noncausal and in fact, oxides with lower tetragonal fraction have been found to be more protective.[26,27] The diffusion of oxygen takes place along the grain boundaries in the oxide layer,[4] the kinetics of which are given by eqn [1]. The size of the columnar grains and their grain-to-grain misorientation (**Figure 6**) have been related to the transition thickness.

Studies of Zircaloy corrosion in autoclaves clearly reveal the cyclic corrosion kinetics,[20,24] the oxide layer appearing to be composed of successive layers of 2–3 μm thickness (**Figures 8–10**), for which the oxidation kinetics progressively decrease as a result of the growth of the oxide layer, in accordance with eqn [1]. The cycles are separated by transitions during which the kinetics appears to accelerate. The transitions are caused by the destabilization of the oxide layer, as a result of which the passivating layer becomes porous and fractured at the end of the cycle, losing its protective role, and reopening for rapid oxidation. A new oxidation cycle then starts. Several processes have been suggested for the destabilization of the oxide layer, such as[7,25–27]:

(a) Cracking of the oxide as a result of the accumulation of compressive stresses in the oxide from imperfect accommodation of the volume expansion attendant upon oxide formation.
(b) Cracking of the oxide as a result of the transformation of initially tetragonal ZrO_2 to the monoclinic modification,[10] or as a result of the oxidation of intermetallic precipitates initially incorporated in metallic form, both of which result in a volume increase.
(c) The porosity formed in the oxide reaches a percolation condition, leading to easy access of the coolant to the underlying metal.

The first factor is normally considered to be the main driver, although the other factors have also been proposed to contribute. The levels of stress accumulation depend on the phase transformation tensor (various levels of accommodation of the Pilling-Bedworth strains in the in-plane directions), which

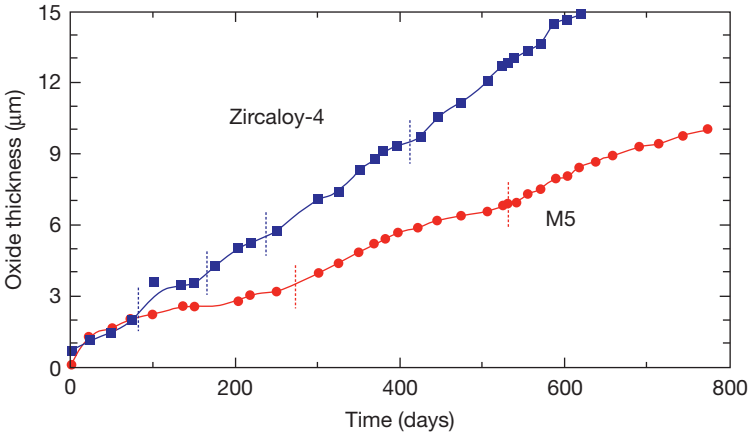

Figure 8 Results of oxidation tests of Zircaloy-4 and of M5™ in autoclaves, at 360 °C, with 10 ppm Li and 650 ppm B, showing the cyclic nature of the oxidation. Redrawn from Bataillon, C.; Féron, D.; Marchetti, L.; *et al*. E-DEN Monograph ''Corrosion'' Commissariat à l'Énergie Atomique; 2008.

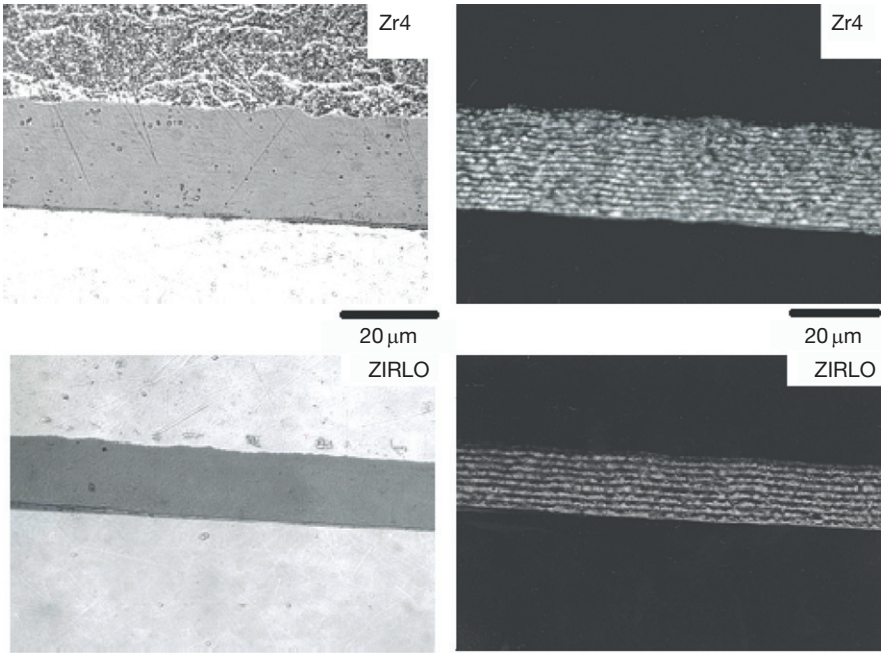

Figure 9 Optical micrographs of oxide layers formed in Zircaloy-4 and in ZIRLO™, in reflected (left) and transmitted light (right). The regular periods formed during the cyclic corrosion process correspond to the oxide transitions in the two alloys. Photo courtesy of G. Sabol, Westinghouse Electric Co.

has been shown to vary from alloy to alloy, thus likely causing the consistent differences seen among the oxide thicknesses at transition for various alloys. Thus, each alloy has a reproducible transition thickness in a given environment. This cyclic process has been shown to reproduce itself with remarkable regularity upward of 17 transitions,[26,27] as shown in **Figure 9**. This can also be seen in the SEM micrograph in **Figure 10** which suggests that cracking occurs at transition.

As discussed by Battaillon *et al*.,[25] the kinetics of the cyclic process can be described by a succession of equations similar to [1] and [2], each representing a specific cycle. The length of the cycle seems to be material dependent as shown in **Figure 8**. Also, Zircaloy contains second phase precipitates of Zr(Cr, $Fe)_2$ and tin as a dissolved element (see **Chapter 2.07, Zirconium Alloys: Properties and Characteristics**). The intermetallic precipitates are known to have a

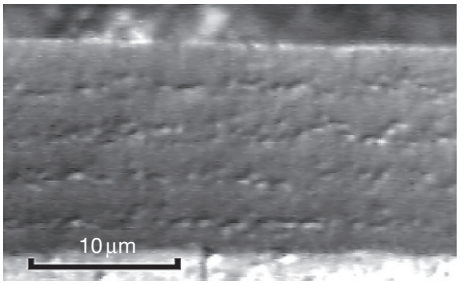

Figure 10 The oxide layer formed on M5™ in autoclaves at 360 °C, with 10 ppm Li and 650 ppm B dissolved in the water showing the layered nature of the oxide, with periodic cracking. Bataillon, C.; Féron, D.; Marchetti, L.; *et al.* E-DEN Monograph ''Corrosion'' Commissariat à l'énergie atomique, 2008. From DEN Monographs ''Corrosion and Alteration of Nuclear Materials,'' ISBN 978-2-281-11369-3 (2010), éditions du Moniteur, © CEA.

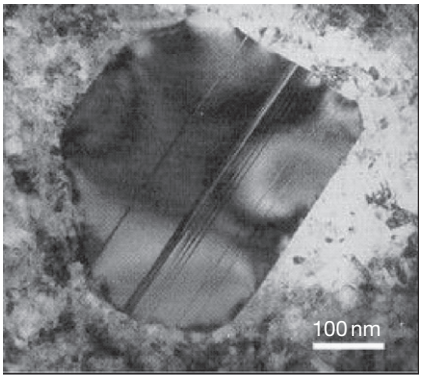

Figure 11 $Zr(Cr,Fe)_2$ precipitates incorporated in metallic form into the oxide layer on Zircaloy-4. Adapted from Pecheur, D.; Lefebvre, F.; Motta, A. T.; Lemaignan, C.; Charquet, D. Oxidation of Intermetallic Precipitates in Zircaloy-4: Impact of Irradiation. In *10th International Symposium on Zirconium in the Nuclear Industry*, ASTM STP 1245; Baltimore, MD, 1994; 687–70; Pecheur, D.; Lefebvre, F.; Motta, A. T.; Lemaignan, C.; Wadier, J. F. *J. Nucl. Mater.* **1992**, *189*, 2318–332.

higher oxidation resistance than the zirconium matrix.[28,29] When the oxidation of the zirconium progresses, the $Zr(Cr,Fe)_2$ precipitates are incorporated in metallic form into the oxide layer (**Figure 11**). However, the iron is progressively dissolved in the zirconium oxide. Tin is present in the oxide layer as nanoparticles of β-Sn, SnO, or $Sn(OH)_2$. The slower oxidation kinetics of Zr–Nb alloys have been attributed to the absence of the second phase precipitates.[7]

5.03.3.2 Temperature and Heat Flux

An increase of temperature increases the oxidation kinetics, as is evident from eqn [1], and confirmed

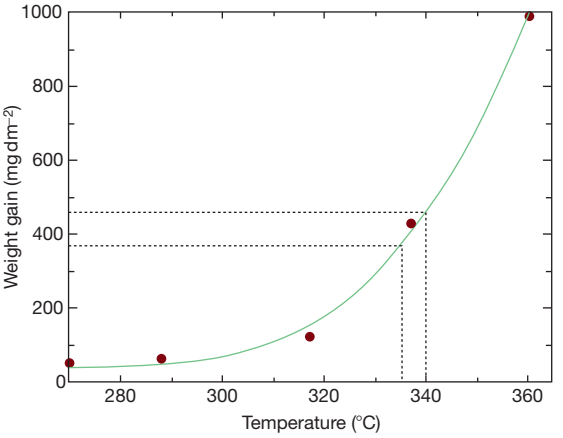

Figure 12 The effect of temperature on the oxidation kinetics of Zircaloy-4, as derived from autoclave test in water for 2500 days. Reproduced from Hillner, E.; Franklin, D. G.; Smee, J. D. J. Nucl. Mater. 2000, 278, 334.

experimentally. As shown in **Figure 12**, the corrosion kinetics accelerate above about 310 °C. An increase of 5 °C for a typical cladding temperature of 335 °C results in a 26% increase in weight gain.

The temperature of the metal–oxide interface (T_i) is, however, not only dependent on the temperature of the coolant, but also on the heat flux (ϕ in W cm^{-2}):

$$T_i \approx T_s + \frac{\phi e}{\lambda}$$

where T_s is the temperature at the water–oxide layer boundary, e the oxide layer thickness (in cm), and λ the thermal conductivity of the oxide layer (W cm^{-1} K^{-1}). Considering that zirconium oxide is a poor thermal conductor, the oxide layer will act as an insulator increasing the temperature of the metal–oxide interface. For typical values for a PWR ($\phi = 55$ W cm^{-2}) and a thermal conductivity of 0.022 W cm^{-1} K^{-1}, the interface temperature increases 1 K for an oxide layer of 4 µm.[25]

As a related effect, nucleate boiling can occur at the oxide–water boundary, once this boundary reaches the saturation temperature (344.5 °C at 15.5 MPa in a PWR). As a result, an enrichment of Li in the liquid phase near the oxide–water boundary can occur (**Figure 13**), which can reach a factor of 3.[25] This is not expected to increase the corrosion significantly for conditions typical for PWRs.

5.03.3.3 Coolant Chemistry

The corrosion of Zircaloy is influenced by the chemical composition of the coolant. The PWR coolant

contains boron and lithium. Boron, present as boric acid (1000–2000 ppm at the beginning of the cycle, depending on the cycle length, and about zero at the end of the cycle), is added to control the core reactivity through neutron absorption of ^{10}B. The boric acid is weakly dissociated, particularly at high temperature, which could lead to a slightly acidic environment. To counteract this, small quantities of lithium hydroxide (5–10 ppm) are added in the water, to obtain a slightly alkaline pH, to avoid deposition of corrosion products on the cladding and limit the corrosion of core structures made of stainless steel or Inconel alloys. (Lithium enriched over 99% of ^{7}Li is used, as the use of ^{6}Li produces the undesirable tritium through activation.) In addition, the coolant may contain small concentrations of anionic impurities that play a role in the corrosion mechanism (**Figure 14**).

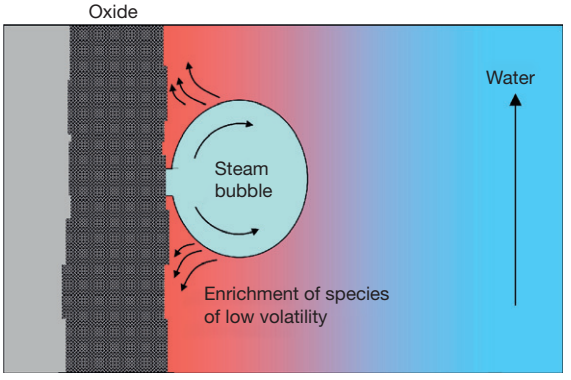

Figure 13 Schematic representation of the enrichment of species at the oxide–water boundary during nucleate boiling. Adapted from DEN Monographs ''Corrosion and Alteration of Nuclear Materials,'' ISBN 978-2-281-11369-3 (2010), éditions du Moniteur, © CEA.

Extensive research has been performed to understand the role of lithium hydroxide and boric acid on the kinetics of the corrosion of zirconium alloys. Experiments in autoclaves have shown that the rate of oxidation of Zircaloy-4 increases significantly when boric acid is absent.[25] After an initial stage where the corrosion kinetics are as expected, corrosion is accelerated in conjunction with a decrease of the thickness of the protective oxide layer,[30,31] as derived from microscopic observations, especially by the ingress of Li into the oxide (**Figure 15**). Enhanced dissolution of the crystallite grain boundaries has been suggested as the mechanism.[32] This effect was absent in the presence of boric acid, and no significant difference was observed for the oxidation kinetics for LiOH concentrations between 70 and 1.5 ppm (**Figure 14**). The protective effect of boric acid has been suggested to be related to the plugging of the porosity in the oxide by a borate compound.[33]

The coolant chemistry also influences the solubility of coolant-borne metallic impurities (e.g., iron, nickel, copper, etc. arising from corrosion release from circuit surfaces), which may deposit on fuel rod surfaces as CRUD, which is composed of metal oxides such as Fe_2O_3 (hematite), Fe_3O_4 (magnetite), FeOOH (goethite), or $(Ni,Co)_xFe_{3-x}O_4$ (spinel).[34–36] Such CRUD deposits are occurring specifically at positions with sub-cooled boiling and may have, in some cases, appeared to contribute to accelerated

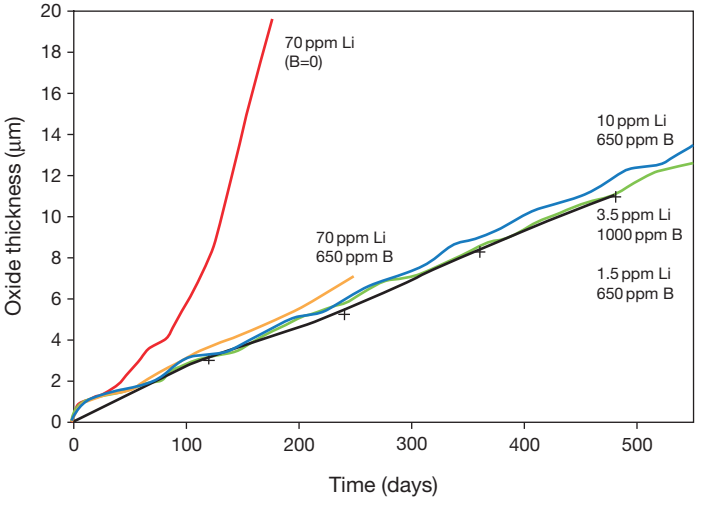

Figure 14 The effect of Li and B on the oxidation kinetics of Zircaloy-4. Bataillon, C.; Féron, D.; Marchetti, L.; *et al*. E-DEN Monograph ''Corrosion'' Commissariat à l'Énergie Atomique, 2008. From DEN Monographs ''Corrosion and Alteration of Nuclear materials,'' ISBN 978-2-281-11369-3 (2010), éditions du Moniteur, © CEA.

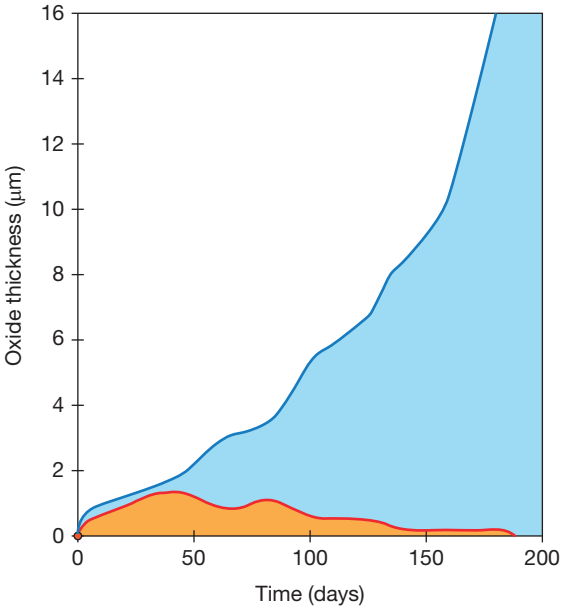

Figure 15 The evolution of the microstructure of the oxide layer on Zircaloy-4 after oxidation in an autoclave with 70 ppm Li, without boron (360 °C). The blue line shows the total oxide thickness, whereas the red line shows the thickness of the protective inner layer. Reproduced from Bataillon, C.; Féron, D.; Marchetti, L.; *et al*. M. E-DEN Monograph ''Corrosion'' Commissariat à l'Énergie Atomique; 2008.

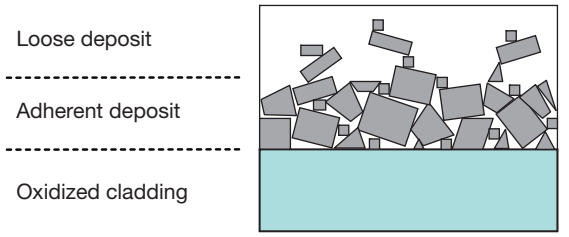

Figure 16 Schematic representation of the CRUD morphology.

oxidation of both BWR and PWR cladding. CRUD can have a wide variety of morphologies, from dense to porous, thus having very different thermal conductivity. The CRUD structure can generally be described an inner deposit that is tightly adherent to the oxide layer and an outer deposit that has a loose structure (Figure 16). However, the thermal conductivity of CRUD is generally better than that of zirconium oxide and therefore its added effect on deterioration of the heat flux through the corrosion layer rarely results in excessive cladding temperatures. Because the lithium concentration in the CRUD, where it is deposited as lithium borate, is increased significantly above the coolant's nominal level, the increased corrosion caused by CRUD deposits is thought to be due to the role of Li, in combination with the increased metal/oxide interface temperature.[37]

Fluorine is produced in the coolant water by neutron capture in ^{18}O to give ^{19}F. Laboratory experiments have shown that the corrosion of Zircaloy-4 begins to accelerate between 19 and 190 ppm fluorine at 360 °C, which is well above the coolant specification in most reactors (0.15 ppm).

5.03.3.4 Irradiation Effects

A wealth of information exists on the in-reactor behavior of Zircaloy from worldwide fuel monitoring programs as well as from experimental research programs, from which information about the radiation effects on zirconium alloy corrosion can be deduced. These effects can be of multiple origin and include radiolysis of the coolant, changes in the metallurgical condition, displacement damage, or phase transformations. As discussed by Cox,[7] no in-reactor effects are evident for an oxide layer thickness below 5–6 μm. Above that thickness, a departure from data with radiation field and for in-reactor conditions suggests an irradiation-induced acceleration of the oxide breakdown. Bataillon *et al.*[25] suggest a factor of 2 for the oxidation rate of Zircaloy-4 between in-reactor and autoclave experiments during the first two reactor cycles. This increases to about 4 during cycles 5 and 6. This effect is shown in Figure 17, in which the thickness of the oxide layer on Zircaloy-4 as a function of exposure time is compared for three cases: (a) autoclaves without thermal gradient, (b) corrosion loop with thermal gradient generated by an electrical heating inserted in the cladding tube, and (c) in-reactor, with the effects of thermal gradient and irradiation.[38]

5.03.3.4.1 Radiolysis

The ionizing radiation will interact with water molecules producing a variety of reaction products:

$$H_2O \xrightarrow{h\nu} e^{\cdot}, H^{\cdot}, OH^{\cdot}, H_2O_2, H_2$$

Figure 18(a) shows the results of a typical computer simulation of the speciation as a function of time.[15] As one can see, numerous oxidizing species such as O_2, $O^{\cdot}$, HO_2, and H_2O_2 that could accelerate the corrosion are formed. For this reason, the coolant water in PWRs is hydrogenated. This effect is

shown in Figure 18(b), which indicates that the presence of hydrogen significantly reduces the steady-state concentration of the oxidizing species.

5.03.3.4.2 Irradiation effects in the oxide layer

Because the growth of the oxide layer on zirconium alloys is strongly related to the diffusion of oxygen ions through the layer, as discussed above, the displacement of ions from their lattice sites by fast neutron damage could lead to enhanced point defect concentrations, enhanced diffusion, and hence enhanced corrosion in-reactors.[39,40] However, experimental studies have shown no clear evidence for this.

Formation of electron–hole pairs and Compton electrons by β and γ radiation could also theoretically lead to a significant increase in the electron conduction (electrical conductivity). The experimental evidence for this is, however, not conclusive.

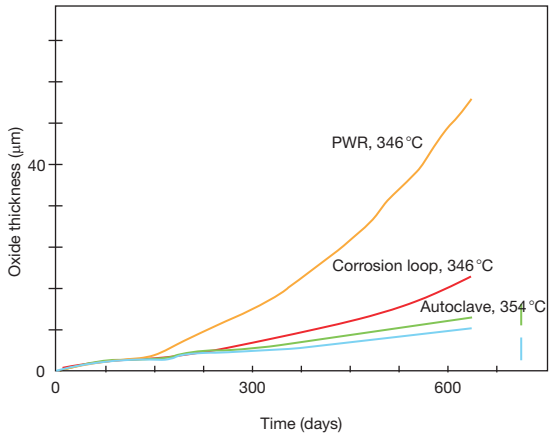

Figure 17 The thickness of the oxide layer on Zircaloy-4 as a function of exposure time for three cases: (a) autoclaves without thermal gradient, (b) corrosion loop with thermal gradient generated by an electrical heating inserted in the cladding tube, and (c) in-reactor, with the effects of thermal gradient and irradiation. Reproduced from Gilbon, D.; Bonin, B. E_DEN Monograph ''Les Combustibles Nucléaires,'' Commissariat à l'Énergie Atomique; 2008.

5.03.3.4.3 Changes in the metallurgical state of the metal

Fast neutron irradiation can change the relative concentration of alloying elements between precipitate and matrix by a variety of mechanisms including ballistic mixing by a primarily knock-on effect.[41] Fe and Cr can be dissolved from the intermetallic $Zr(Cr, Fe)_2$ particles into the surrounding α-Zr matrix.[42,43] The dissolution is linked to precipitate amorphization and the modified equilibrium between the amorphous precipitate and the matrix.[44] As a result of the precipitate dissolution, the smallest particles dissolve completely, and the largest are significantly reduced in size. The ultimate location of the Fe is determined by thermal diffusion effects in the vicinity of the intermetallic particles where c-type dislocations may have formed. Postirradiation[45] corrosion of such specimens shows progressive

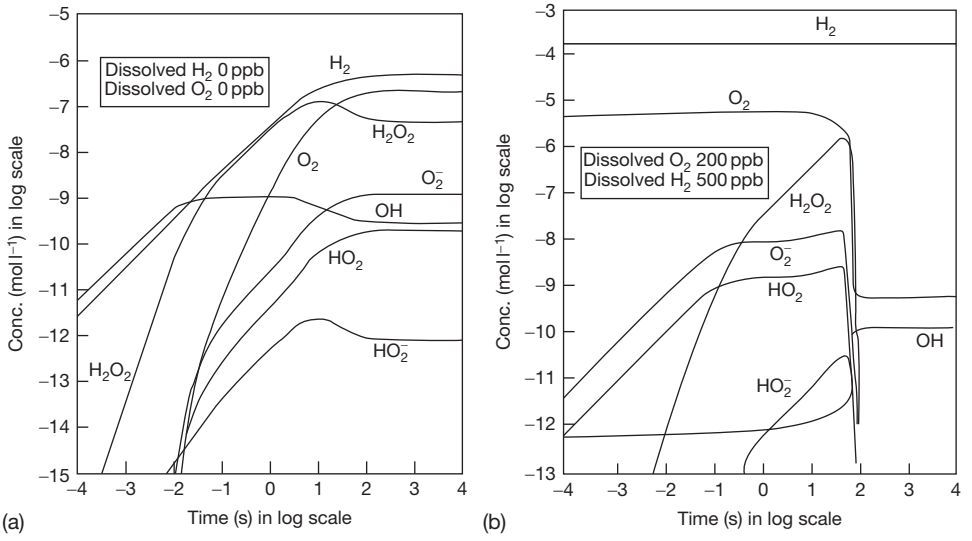

Figure 18 Typical result of a computer simulation or radiolysis of water at 250 °C for a dose rate of 4.5×10^2 Gy h^{-1}; (a) pure water; (b) with dissolved O_2 and H_2. Reproduced from Waterside Corrosion of Zirconium Alloys in Nuclear Power Plants; IAEA-TECDOC-996; International Atomic Energy Agency, Vienna, Austria, 1998.

degradation of the posttransition corrosion rates with increasing dose, although other studies have shown nodular corrosion improvement of irradiated material.[46] Cox[7] concluded that this effect is now seen as a primary contributor to enhanced corrosion in PWRs, since alloys that do not contain Fe or in which the Fe is incorporated in radiation-resistant particles, show lower in-reactor corrosion kinetics.

5.03.4 Nodular Oxidation

In BWR conditions (**Table 1**), nonuniform, so-called nodular oxidation can also take place (**Figure 19**). The mechanism for nodular oxidation is yet to be fully understood, as it has proved to be challenging to study in laboratory experiments. Oxidation studies in 500 °C steam demonstrated the dependence of nodular corrosion on second phase precipitate size and distribution,[47] typical for various cladding batches and their metallurgical structure. However, other factors also affect nodule formation, as batches of the same cladding can behave quite differently. Such differences can be related to in-reactor phenomena such as galvanic effects, impurities, radiolytic species, and local power and flux.[7,15] The question of whether nodular corrosion nucleates at intermetallic particles, between intermetallic particles, or as a collective property of a group of grains, is yet to be resolved.[6] As discussed by the IAEA Expert group,[6] the experimental evidence points toward the fact that nodules form away from intermetallic precipitates in the alloys. In his review, Cox[7] concluded that the redistribution of Fe from secondary phase particles diminishes nodular corrosion, but enhances uniform corrosion.

5.03.5 Hydrogen Embrittlement

Absorption of hydrogen is a major contributor to degradation of zirconium alloys during service in nuclear systems.[22] This degradation is primarily attributed to the formation of zirconium hydrides, a brittle phase that can embrittle cladding, and reduce its fracture toughness, thus enhancing the susceptibility to cracking.[48] Recent studies have also shown that the addition of hydrogen can increase the creep rates in Zr–2.5Nb[49] and possibly irradiation growth.

The hydrogen can come from a variety of sources, some of them detailed in a 1998 report from an IAEA Expert group[14]:

(i) Hydrogen left over in the Zircaloy tubing after fabrication or from residual moisture due to surface preparation (the initial concentrations of hydrogen in the cladding, postfabrication but prereactor service, are on the order of 10 wt ppm).
(ii) Desorption of water from incompletely dried up fuel.
(iii) Hydrogen produced by (n,p) reactions in the cladding.
(iv) Hydrogen ingress from the coolant water into the cladding during reactor exposure.

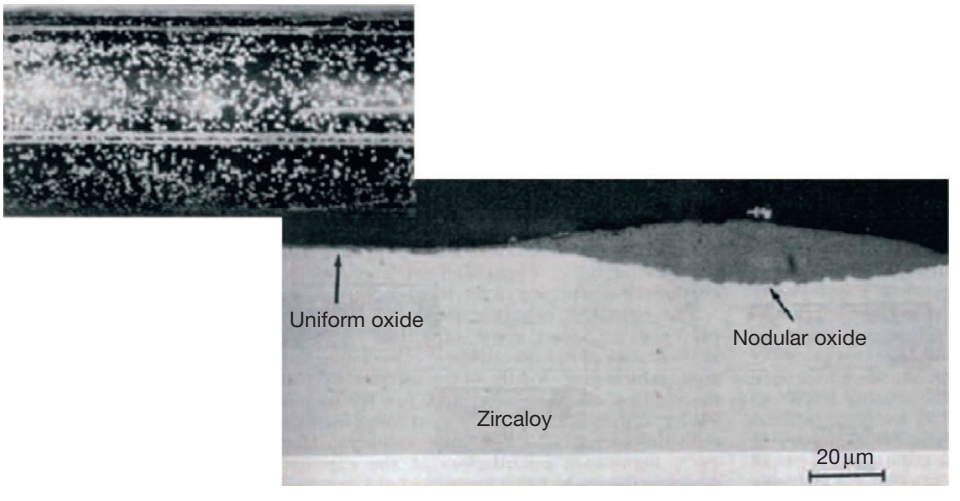

Figure 19 Typical appearance of nodular corrosion in visual inspection and metallographic examination. Figures courtesy of Ron Adamson.

(v) Absorption during the normal corrosion processes that occur in high-temperature aqueous solutions.

(vi) Direct reaction of a clean (no species other than zirconium) surface with gaseous hydrogen. This hydrogen nominally could come from three sources: protons released by oxidation that form hydrogen gas, hydrogen produced by radiolysis of the water exposed to a high-energy neutron flux, and hydrogen specifically added to the cooling water to control stress corrosion cracking (see **Chapter 5.02, Water Chemistry Control in LWRs** and **Chapter 5.08, Irradiation Assisted Stress Corrosion Cracking**).

(vii) Diffusion of hydrogen through a metallic bond with a dissimilar metal in which hydrogen has a higher activity.

(viii) Cathodic polarization of zirconium in an electrolyte (typical for low-temperature reactors).

By far, the largest source comes from the normal corrosion processes (v).

5.03.5.1 Hydrogen Production During Aqueous Corrosion of Zirconium-Base Materials

The reaction of Zr with water to form zirconium oxide produces atomic hydrogen (a proton)

$$Zr + 2H_2O \rightarrow ZrO_2 + 2H_2 \qquad [Ia]$$

$$Zr + 2H_2O \rightarrow ZrO_2 + 4H \qquad [Ib]$$

The proton released in the oxidation of Zr either combines with another proton to form gaseous hydrogen (eqn I(a)) or diffuses into the zirconium (eqn I(b)), where it can form zirconium hydrides. The majority of the protons formed during oxidation combine to form hydrogen gas but a fraction enters the metal. The term 'hydrogen pickup fraction' f_H is used to relate the hydrogen absorbed to the hydrogen liberated during the corrosion reaction.

$$f_H = \frac{\text{H absorbed in cladding}}{\text{H generated in corrosion}}$$

Although the total amount of hydrogen absorbed is proportional to oxide thickness, the proportionality constant, the hydrogen pickup fraction, changes from alloy to alloy such that alloy design can significantly improve cladding performance. The pickup fraction also changes with corrosion temperature and with corrosion time, but the mechanisms by which this occurs are not yet resolved.

5.03.5.2 Hydrogen Absorption

A detailed overview of the process of the absorption of hydrogen into zirconium-base materials is provided in the IAEA Technical Document 'Waterside Corrosion of Zirconium Alloys in Nuclear Power Plants.'[15] The oxide itself generally presents an effective barrier to the absorption of hydrogen such that the structure of the oxide and the electron transport mechanism can be linked to hydrogen uptake. There is some evidence that the nickel content in Zircaloy-2 increases the absorption of hydrogen (**Figure 20**), either by supporting direct dissociation of water or by mitigating recombination of hydrogen and oxygen.[50–52] This was one reason why the nickel was removed in the formulation of Zircaloy-4. The Zr $(Fe,Ni)_2$ intermetallic particles that exist in Zircaloy may provide a significant pathway for hydrogen uptake. Specifically, the electron current flows primarily at sites where intermetallic particles partially, or completely, short-circuit the oxide.[53] Additionally, flaws have been found to exist in the oxide that are not associated with existing intermetallic particles but are at pits that may have resulted from intermetallic dissolution during pickling. These flaws allow the cathodic process to proceed. These locations are evidenced by cracks or small holes visible in the oxide.[54]

For some alloys, the amount of absorbed hydrogen varies as a function of oxide thickness. For example, Cox[55] has shown that for Zircaloy-2, an initially high hydrogen absorption rate decreases as the oxide thickness increases, but then picks up again after the oxide reaches the transition region. Other researchers have shown an increase in H uptake just *before* the oxide transition.[56] The additional porosity in the oxide, after transition, makes hydrogen pickup more likely. For Zircaloy-4, the pickup appears to be constant with the growth of the oxide. Oxygen additions to the water normally reduce the hydrogen uptake and hydrogen additions increase it.[57]

5.03.5.3 Hydride Formation

Hydrogen absorbed into the zirconium alloy cladding at levels more than the terminal solid solubility can embrittle the cladding through the formation of hydrides. The stress concentration at the ends of

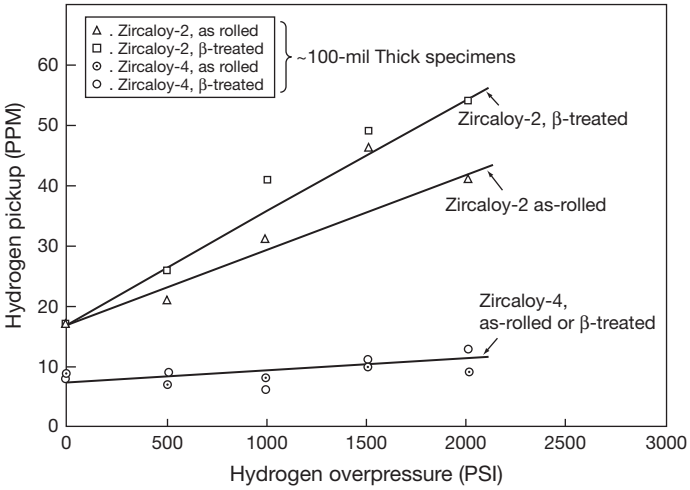

Figure 20 Hydrogen pickup in Zircaloy-2 and Zircaloy-4 as a function of hydrogen overpressure after 14 days in 343 °C water. Reproduced from Hillner, E. Hydrogen absorption in Zircaloy during aqueous corrosion, Effect of Environment, U.S Rep. WAPD-TM-411, Bettis Atomic Power Lab., W Mifflin, PA, 1964.

larger plate-type hydrides, as well as the localized deformation in the ligaments between the hydrides, leads to material weakness. As confirmed by Kerr *et al.*,[58] performing recent *in situ* fracture work at the Advanced Photon Source at Argonne National Laboratory, in materials with large pregrown hydrides (~100 μm), the residual stress field of the zirconium matrix governs the residual stress state of the hydride and load is shed to the notch tip hydride phase on increasing applied load.

The hydrides, if formed, can be circumferential or radial (see **Figure 21**). The embrittlement is influenced by the orientation of hydrides relative to the stress. Hydrides that are oriented normal to the tensile load enhance embrittlement by providing an easy path for the growth of cracks through the hydrides.[59] Radial hydrides are of greater concern, as they are oriented perpendicular to the hoop stress that arises during operation of the cladding tube. As one example, the stress ratio (hoop stress/axial stress $= \sigma_\theta/\sigma_z$) from gas pressurization anticipated during a loss of coolant accident has an approximate value of two and most of the deformation is in the hoop direction.[60]

The hydrides observed in fuel cladding exposed to reactor environment are most often fcc delta hydrides ZrH_x (where $x \sim 1.6$). For a fixed amount of hydrogen uptake, the density and size of the formed hydrides is a strong function of the material microstructure. Initial hydride orientation has been shown to be a function of the texture of the Zircaloy-4 that develops during fabrication.[61,62] As an example, as reported by Singh and coworkers,[63] Zr–2.5Nb that has been quenched and aged forms a higher density of smaller hydrides than Zr–2.5Nb that was cold-rolled and stress relieved, and the difference was attributed to the underlying grain structure, which acted as the nucleation host for the formation of hydrides. If sufficient stress is applied during the formation of the hydrides, the hydride platelets will form perpendicular to the applied stress.

A specific example of deleterious hydride orientation is from 'DHC,' in which circumferentially oriented hydrides dissolve and reprecipitate at the crack tip, parallel to the crack orientation. Understanding DHC is of specific concern for CANDU pressure tubes and ensuring the long-term stability of spent fuel during storage and is discussed later in this section.[64–69]

5.03.5.4 Hydride Formation Rates

At reactor operating temperatures, the stable phases in the Zr–H phase diagram are (i) hcp-Zr with dissolved hydrogen and the delta hydride ZrH_x, where x varies between 1.45 and 1.2 at high temperature. The terminal solid solubility of H in hcp-Zr is

$$C^{H}_{\alpha-Zr} = A\exp(-E_H/T) \qquad [5]$$

where A is a constant equal to 1.2×10^5 wt ppm (or 0.8 mole H per cm^3), and the activation energy for solid solution is 4300 K (the temperature validity for this equation is up to 865 °C, the limit of the alpha phase region).

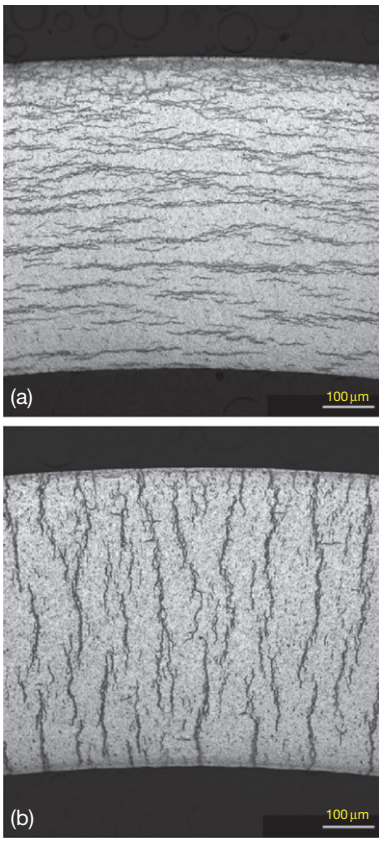

Figure 21 (a) Circumferential and (b) radial hydrides. Figures courtesy of Ron Adamson.

Hydrogen is very mobile in α-Zr and once it is absorbed in the cladding, it migrates easily in response to concentration, temperature, and stress gradients. The diffusion coefficient of H in Zr is

$$D_{\mathrm{Zr}}^{\mathrm{H}} = D_0^{\mathrm{H}} \exp(-E_{\mathrm{m}}^{\mathrm{H}}/k_{\mathrm{B}}T) \qquad [6]$$

where $E_{\mathrm{m}}^{\mathrm{H}} = 0.47\mathrm{eV}$ and the preexponential factor is $7 \times 10^{-3}\,\mathrm{cm}^2\,\mathrm{s}^{-1}$. This results in a high diffusion coefficient at the reactor operating temperatures (at 355 °C (average cladding temperature), the diffusion coefficient is $1.1 \times 10^{-6}\,\mathrm{cm}^2\,\mathrm{s}^{-1}$), so that hydrogen responds quickly to changed conditions to establish a new steady state. The characteristic time to attain significant hydrogen ingress by diffusion through the thickness of the cladding at this temperature is about 12 min, which is much smaller than normal reactor exposure times. This means that at any given time, the hydrogen distribution in the cladding can be considered to be in quasi-steady state, that is, temporal variations need not be considered. Because of this, when the hydrogen is in solid solution (before hydride precipitation), the hydrogen concentration in the cladding is essentially homogeneous.

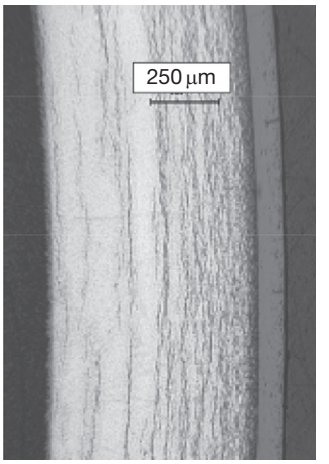

Figure 22 Hydride-rim formation in cladding on high-burnup (67 GWd/t) PWR fuel. (cladding from the H. B. Robinson plant, courtesy R. Daum ANL).

5.03.5.5 Formation of Hydride Rim

As, from eqn [5], the hydrogen solubility in Zircaloy decreases with decreasing temperature, the outer cladding arrives at the solubility limit before the inner cladding does. For an outer cladding temperature of 325 °C and an inner cladding temperature of 385 °C, the hydrogen solubilities are respectively 90 and 170 wt ppm. This causes hydrides to form preferentially at the outer cladding diameter.

Metallographic examinations performed on cladding hydrided below the solubility limit show a more or less homogeneous hydride distribution through the thickness of the cladding. These hydrides presumably have precipitated out during the cooling from operation temperature, so that at reactor temperature, the hydrogen is in solution.

As the overall hydrogen content increases as a result of increased corrosion, eventually the outer layer of the cladding reaches saturation and a hydride rim starts to form, whose thickness will increase with increasing reactor exposure. Figure 22 shows a metallograph of high-burnup cladding showing enhanced hydride formation near the outer diameter of the cladding.

The hydride distribution response to stress and temperature gradients is at the root of several degradation mechanisms, such as DHC, secondary hydriding, and the degradation of cladding ductility from oxide spalling.

5.03.6 Delayed Hydride Cracking

A detailed summary of the DHC phenomena is available in the report of an IAEA (International Atomic Energy Agency) Coordinated Research Project.[70] An overview is presented here.

The classic theory of DHC comes from the work of Dutton and Puls.[71] The basis of the Dutton and Puls' theory is sketched in **Figure 23**. The basis of the theory is that the crack tip hydride grows as hydrogen migrates from hydrides in the bulk of the material to the crack tip. The driving force for the diffusion of the hydrogen is the difference in the chemical potential of hydrogen between the bulk material and the crack tip hydride in response to hydrostatic stress.[70,72]

Dutton and Puls' theory follows the following logic. The partial molar volume of hydrogen in the hydrides is positive. An increasing hydrostatic tensile stress reduces the chemical potential of hydrogen in the hydride relative to the bulk. This chemical potential difference causes hydrogen in solution to diffuse to the crack tip where it precipitates. In this model, the hydrides in the bulk dissolve to maintain the hydrogen concentration at the hydride interface at the solubility limit for the temperature at which the cracking is occurring. As the precipitate grows at the crack tip, it will eventually reach a critical size that is dependent on the stress intensity factor at the crack tip and the crack will then progress an additional distance that is related to the hydride size. The relationship between crack velocity and stress intensity factor for this type of cracking is shown in **Figure 24**. The stable crack growth velocity is a function of temperature since that temperature affects both hydrogen solubility and hydrogen transport to the crack tip.

A detailed update of the Dutton-Puls' theory, along with a response to challenges to the theory by the group of Kim[73] was recently released.[74] The review by McRae supports the validity of the Dutton and Puls' models rather than the alternatives promoted by Kim.

Recently, Colas *et al.*[75] used high-energy synchrotron X-rays at the advanced photon source, to perform *in situ* characterization of hydride dissolution, reprecipitation, and reorientation during thermal cycles under load. Their results, from samples initially charged with hydrogen at concentrations up to 600 ppm, indicate that the reorientation occurred above a threshold stress of 75–80 MPa. In another

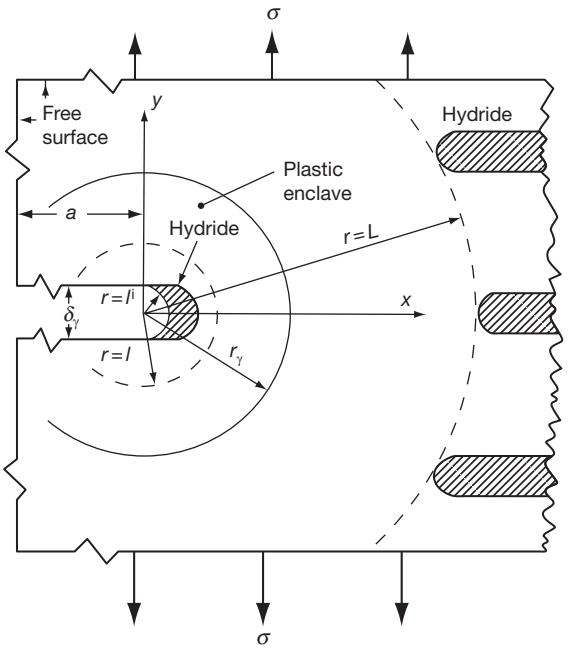

Figure 23 Crack and diffusion geometry assumed in the DHC model of Puls. Reproduced from Puls, M. P. *J. Nucl. Mater.* **2009**, *393*, 350–367.

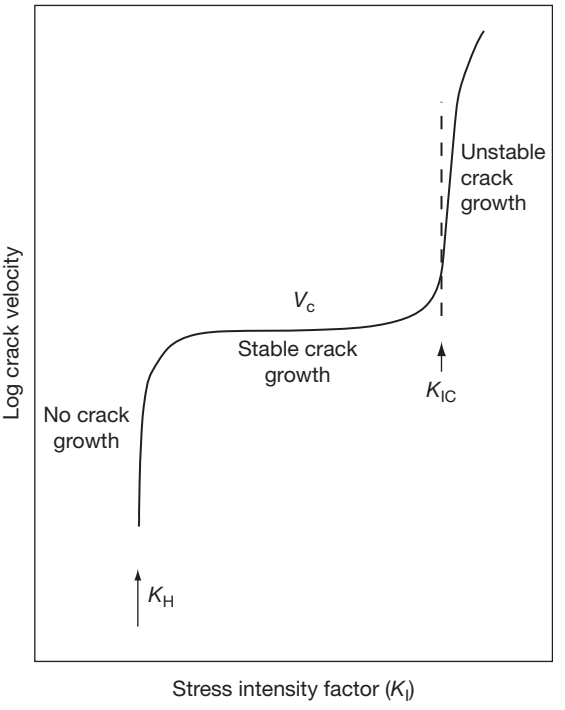

Figure 24 Schematic diagram of crack propagation by DHC in hydrided Zircaloy. Reproduced from Delayed hydride cracking in zirconium alloys in pressure tube nuclear reactors. IAEA-TECDOC-1410; Nuclear Power Technology Development Section, International Atomic Energy Agency, Vienna, Austria, 2004.

recent study related to hydride reorientation, Daum *et al.*[76] found that the threshold stress is approximately 75–80 MPa for both nonirradiated and high-burnup stress-relieved Zry-4 fuel cladding cooled from 400 °C. Within the uncertainty of the experiment, the irradiation was not critical to setting the threshold stress. Under ring compression at both room temperature and 150 °C, Daum found that radial-hydride precipitation embrittles Zry-4. Interestingly, for nonirradiated Zircaloy-4, samples with lower hydrogen concentration (300 vs. 600 ppm) appeared to be more susceptible to radial-hydride related embrittlement. In a separate work, Daum[76] also showed that failure is sensitive to hydride-rim thickness. Zircaloy-4 cladding tubes with a hydride-rim thickness $>100\,\mu m$ ($\approx$700 wt ppm total hydrogen) exhibited brittle behavior, while those with a thickness $<90\,\mu m$ ($\approx$600 wt ppm) remained ductile.

5.03.7 Summary and Outlook

The extensive research on the corrosion of zirconium alloys has resulted in an enormous flow of information during several decades. On the basis of this, a basic understanding of the processes leading to oxidation and hydriding of zirconium alloys now exists.

1. Zirconium alloy fuel cladding undergoes corrosion when subjected to the reactor environment. The corrosion is related to the oxidation of the metal by coolant water and is associated with hydrogen uptake into the cladding. The latter phenomenon is the main contributor to in-reactor degradation of cladding performance.
2. Uniform corrosion is alloy dependent and environment dependent. The higher fuel duty now imposed on nuclear fuel can lead to accelerated corrosion, which can limit fuel lifetime.
3. Corrosion is accelerated under irradiation relative to out-of-pile results. The corrosion rates can increase after a given exposure.
4. The hydrogen pickup fraction can vary from alloy to alloy and for different environments and corrosion times. The hydrogen pickup mechanisms and the influence of the alloy on the process are still under study.
5. Modern alloys such as M5 and ZIRLO provide much improved corrosion performance and show the potential for significant benefits from careful alloy design.

Many challenges remain to be addressed in understanding the corrosion and hydriding of Zr alloys in nuclear environments. Although mechanistic understanding has been developed over the past decades, still much needs to be understood, in particular, on the role of alloy design on corrosion rate, hydrogen pickup, and oxide transition. In addition, the behavior of cladding under the more challenging conditions of severe fuel duty associated with longer exposures, higher temperatures, aggressive chemistry, and incidence of boiling needs to be studied.

References

1. Kestersson, R.; Yueh, K.; Shah, H.; *et al.* In *2006 International Meeting LWR Fuel Performance (Top Fuel 2006)*, Salamanca, Spain, 2006; pp 67–71.
2. Bossis, P.; Pecheur, D.; Hanifi, K.; Thomazet, J.; Blat, M. *J. ASTM Int.* **2006**, *3*, paper IDJAI 12404.
3. Sabol, G. P. ZIRLO: an alloy development success. In *14th ASTM International Symposium on Zr in the Nuclear* Industry, STP 1467, Stockholm, 2005; pp 3–24.
4. Yang, R.; Ozer, O.; Rosenbaum, H. In *Light Water Reactor Fuel Performance Meeting*; ANS: Park City, UT, 2000.
5. Cox, B. *J. Nucl. Mater.* **1968**, *28*, 1.
6. Cox, B. In *Advances in Corrosion Science and Technology;* Fontana, M. G., Staehle, R. W., Eds.; Plenum: New York, 1976; Vol. 5, p 173.
7. Cox, B. *J. Nucl. Mater.* **2005**, *336*, 205.
8. Lim, D.; Graham, N. A.; Northwood, D. O. The degradation of zirconium alloys in nuclear reactors – a review; Canadian Report, Atomic Energy Control Board, Ottawa (Now Canadian Nuclear Safety Commission) INFO-0174; Jan 1986.
9. Lemaignan, C.; Motta, A. T. Zirconium Alloys in Nuclear Applications, Materials Science and Technology, vol. 10. Nuclear Materials Pt. 2; Frost, B. R. T., Ed.; VCH Verlagsgesellschaft mbH, Weinheim, Germany, 1994.
10. Franklin, D. G.; Lang, P. G. In *9th International Symposium on Zirconium in the Nuclear Industry*, ASTM STP 1132, 1990; pp 3–32.
11. Bailly, H.; Ménessier, D.; Prunier, C., Eds. The Nuclear Fuel of Pressurized Water Reactors and Fast Reactors: Design and Behaviour, Collection du Commissariat á L'Énergie Atomique; English Edition: Intercept, Andover, Hants, UK, 1999.
12. Cox, B. *J. Nucl. Mater.* **1969**, *29*, 50.
13. Cox, B.; Pemsler, J. P. *J. Nucl. Mater.* **1968**, *28*, 73–78.
14. Corrosion of zirconium alloys in nuclear power plants; IAEA TECDOC-684; International Atomic Energy Agency, Vienna, Austria, Jan 1993.
15. Waterside Corrosion of Zirconium Alloys in Nuclear Power Plants; IAEA-TECDOC-996; International Atomic Energy Agency, Vienna, Austria, 1998.
16. Garde, A. M.; Smith, G. P.; Pirek, R. C. Effects of hydride precipitate localization and neutron fluence on the ductility of irradiated Zircaloy-4. In *11th International Symposium on Zr in the Nuclear Industry*, STP 1295, Garmisch-Partenkirchen, ASTM, 1996; pp 407–430.
17. Pierron, O. N.; Koss, D. A.; Motta, A. T.; Chan, K. S. *J. Nucl. Mater.* **2003**, *322*, 21–35.
18. Raynaud, P. R.; Motta, A.; Koss, D. A.; Chan, K. S. Fracture toughness of hydrided Zircaloy-4 sheet under

through-thickness crack growth conditions. In *15th International Symposium on Zr in the Nuclear Industry*, ASTM STP 1505, Sunriver, OR 2007; pp 163–177.
19. Daum, R. S.; Majumdar, S.; Bates, D. W.; Motta, A. T.; Koss, D. A.; Billone, M. C. On the embrittlement of Zircaloy-4 under RIA-relevant conditions. In *Thirteenth International Symposium on Zirconium in the Nuclear Industry*, ASTM STP 1423, 2002; pp 702–718.
20. Motta, A. T.; Gomes-da-Silva, M. J.; Yilmazbayhan, A.; Comstock, R. J.; Cai, Z.; Lai, B. *J. ASTM Int.* **2008**, *5*; paper ID# JAI10125.
21. Kass, S. *J. Nucl. Mater.* **1969**, *28*, 315–321.
22. Bossis, P.; Lelievre, G.; Barberis, P.; litis, X.; LeFebvre, F. Multi-scale characterisation of the metal–oxide interface of zirconium alloys. In *12th Internation Symposium on Zr in the Nuclear Industry*, ASTM STP-1354, 2000; pp 918–940.
23. Hillner, E.; Franklin, D. G.; Smee, J. D. *J. Nucl. Mater.* **2000**, *278*, 334.
24. Bryner, J. S. *J. Nucl. Mater.* **1979**, *82*, 84.
25. Bataillon, C.; Féron, D.; Marchetti, L.; *et al.* E-DEN Monograph ''Corrosion'' Commissariat à l'Énergie Atomique; 2008.
26. Yilmazbayhan, A. PhD. Thesis in Nuclear Engineering, Penn State University, 2004.
27. Yilmazbayhan, A.; Motta, A. T.; Comstock, R. J.; Sabol, G. P.; Lai, B.; Cai, Z. *J. Nucl. Mater.* **2004**, *324*, 6–22.
28. Pecheur, D.; Lefebvre, F.; Motta, A. T.; Lemaignan, C.; Charquet, D. Oxidation of intermetallic precipitates in Zircaloy-4: Impact of irradiation. In *10th International Symposium on Zirconium in the Nuclear Industry*, Baltimore, MD, ASTM STP 1245; 1994; pp 687–705.
29. Pecheur, D.; Lefebvre, F.; Motta, A. T.; Lemaignan, C.; Wadier, J. F. *J. Nucl. Mater.* **1992**, *189*, 2318–2332.
30. Pecheur, D.; Godlewski, J.; Billot, P.; Thomazet, J. Microstructure of oxide films formed during the waterside corrosion of the Zircaloy cladding in lithiated environment. In *11th International Symposium on Zr in the Nuclear Industry*, ASTM STP 1295, Garmisch-Partenkirchen, 1995; pp 94–113.
31. Pecheur, D.; Godlewski, J.; Peybernes, J.; Fayette, L.; Noe, M.; Frichet, A.; Kerrec, O. Contribution to the understanding of the effect of water chemistry on the oxidation kinetics of Zircaloy-4 cladding. In *12th International Symposium on Zr in the Nuclear Industry*; ASTM STP-1354, Toronto, 1998; pp 793–811.
32. Cox, B.; Ungurelu, M.; Wong, Y. M.; Wu, C. In *the 11th International Symposium on Zr in the Nuclear Industry*, ASTM STP 1295; American Society for Testing of Materials, 1996, p 114.
33. Britten, C. F.; Arthurs, J. V.; Wanklyn, J. N. *J. Nucl. Mater.* **1865**, *15*, 263.
34. Roy A. Castelli, Nuclear Corrosion Modelling. The Nature of CRUD. Elsevier ISBN: 978-1-85617-802-0.
35. Orlov, A.; Degueldre, C.; Wiese, H.; Ledergerber, G.; Valizadeh, S. *J. Nucl. Mater*. 2011. doi:10.1016/j.jnucmat.2010.12.033.
36. Janney, D. E.; Porter, D. L. *J. Nucl. Mater.* **2007**, *362*, 104–115.
37. Adamson, R.; Garzarolli, F.; Cox, B.; Strasser, A.; Rudling, P. Corrosion Mechanism in Zirconium Alloys. ZIRAT12 Special Topic Report; ANT International, 2007.
38. Gilbon, D.; Bonin, B. E_DEN Monograph ''Les Combustible Nucléaires'', Commissariat à l'Énergie Atomique; 2008.
39. Maguire, M. A. In *the 9th International Symposium on Environmental Degradation of materials in Nuclear Power Systems*, Newport Beach, CA, 1999.
40. Cox, B.; Alcock, A.; Derrick, F. D. *J. Electrochem. Soc.* **1961**, *108*, 129.
41. Motta, A. T.; Lefebvre, F.; Lemaignan, C. In *the 9th International Symposium on Zr in the Nuclear Industry*, ASTM STP 1132; American Society for Testing of Materials, 1991; p 718.
42. Griffiths, M.; Gilbert, R. W.; Carpenter, G. J. C. *J. Nucl. Mater.* **1987**, *150*, 53.
43. Wang, W. J. S.; Tucker, R. P.; Cheng, B.; Adamson, R. B. *J. Nucl. Mater.* **1986**, *138*, 185.
44. Motta, A. T.; Lemaignan, C. *J. Nucl. Mater.* **1992**, *195*, 277–285.
45. Cheng, B. C.; Kruger, R. M.; Adamson, R. B. In *the 10th International Symposium on Zr in the Nuclear Industry*, ASTM STP 1245; American Society for Testing of Materials, 1994; p 400.
46. Etoh, Y.; Kikuchi, K.; Yasuda, T.; Koizumi, S.; Oishi, M. Neutron irradiation effects on the nodular corrosion on Zircaloy-2. In *International Topical Meeting on LWR Fuel Performance*; American Nuclear Society: Avignon, 1991; pp 691–700.
47. Garzarolli, F.; Stehle, H.; Steinberg, E.; Weidinger, H. Progress in the Knowledge of Nodular Corrosion, ASTM-STP-939; American Society for Testing and Materials: Philadelphia, PA, 1987; p 417.
48. Sawatzky, A.; Ells, C. E. In *Twelfth International Symposium on Zirconium in the Nuclear Industry*, ASTM STP 1354; Sabol, G. P., Moan, G. D., Eds.; American Society for Testing and Materials: West Conshohoken, PA, 2000; pp 32–48.
49. Kishore, R. *J. Nucl. Mater.* **2009**, *385*, 591–594.
50. Hillner, E. Hydrogen absorption in Zircaloy during aqueous corrosion, Effect of Environment, U.S Rep. WAPD-TM-411; Bettis Atomic Power Lab., W Mifflin, PA, 1964.
51. Kass, S.; Kirk, W. W. *ASM Trans. Quart.* **1962**, *56*, 77.
52. Cox, B. The effect of some alloying additions on the oxidation of zirconium in steam, U K. Report, AERE-R4458; United Kingdom Atomic Energy Authority, AERE, Harwell. Berks, 1963.
53. Ramasubramanian, N. *J. Nucl. Mater.* **1975**, *55*, 134–154.
54. Cox, B.; Wong, Y. M. *J. Nucl. Mater.* **1999**, *270*, 134–146.
55. Cox, B. Some factors which affect the rate of oxidation and hydrogen absorption of Zircaloy-2 in steam, U K. Rep. AERE-R4348; United Kingdom Atomic Energy Authority, AERE, Harwell, Berks, 1963.
56. Harada, M.; Wakamatsu, R. *J. ASTM Int.* **2008**, *5*; Paper ID JAI101117.
57. Kass, S. The development of the Zircaloys, Corrosion of Zirconium Alloys, ASTM STP-368; American Society for Testing and Materials, W. Conshohocken, PA, 1964; pp 3–27.
58. Kerr, M.; Daymond, M. R.; Holt, R. A.; Almer, J. D.; Stafford, S.; Colas, K. B. *Scripta Mater.* **2009**, *61*, 939–942.
59. Davies, P. H.; Sterns, C. P. In *Fracture Toughness Testing of Zircaloy-2 Pressure Tube Material with Radial Hydrides Using Direct-Current Potential Drop*; Underwood, J. H., Chait, R., Smith, C. W., Wilhem, D. P., Andrews, W. A., Newman, J. C., Eds.; ASTM STP 905, 1986, p 379.
60. Daum, R. S.; Majumdar, S.; Tsai, H.; *et al.* Mechanical Property Testing of Irradiated Zircaloy Cladding Under Reactor Transient Conditions, Small Specimen Test Techniques, ASTM STP 1418; Sokolov, M. A., Landes, J. D., Lucas, G. E., Eds.; American Society for Testing and Materials: West Conshohocken, PA, 2002; Vol. 4.
61. Vaibhaw, K.; Rao, S. V. R.; Jha, S. K.; Saibaba, N.; Jayaraj, R. N. *J. Nucl. Mater.* **2008**, *383*, 71–77.

62. Kiran Kumar, N. A. P.; Szpunar, J. A.; He, Z. *J. Nucl. Mater.* **2010**, *403*, 101–107.
63. Singh, R. N.; Roychowdhury, S.; Sinha, V. P.; Sinha, T. K.; De, P. K.; Banerjee, S. *Mater. Sci. Eng. A* **2004**, *374*, 342.
64. Marshall, R.; Louthan, M. *Trans. ASM* **1963**, *56*, 693–700.
65. Nagase, F.; Fuketa, T. *J. Nucl. Sci. Technol.* **2004**, *41*(12), 1211–1217.
66. Singh, R.; Kishore, R.; Singh, S.; *et al. J. Nucl. Mater.* **2004**, *325*, 26–33.
67. Choubey, R.; Pulse, M. *Met. Mat. Trans. A* **1994**, *25A*, 993–1004.
68. Barraclough, K.; Beevers, C. *J. Mater. Sci.* **1969**, *4*, 518–525.
69. Daum, R. S.; Majumdar, S.; Liu, Y.; Billone, M. C. *J. Nucl. Sci. Technol.* **2006**, *43*(9), 1054–1067.
70. Delayed hydride cracking in zirconium alloys in pressure tube nuclear reactors. IAEA-TECDOC-1410; Nuclear Power Technology Development Section, International Atomic Energy Agency, Vienna, Austria, 2004.
71. Dutton, R.; Puls, M. P. *Effect of Hydrogen on Behavior of Materials*, TMS-AIME: New York, 1976; pp 512–525.
72. Eadie, R. L.; Coleman, C. E. *Scripta Metall.* **1989**, *23*, 1865–1870.
73. Kim, Y. S. *Mater. Sci. Eng. A* **2010**, *527*, 7480–7483.
74. Puls, M. P. *J. Nucl. Mater.* **2009**, *393*, 350–367.
75. Colas, K. B.; Motta, A. T.; Almer, J. D.; *et al. Acta Mater.* **2010**, *58*, 6575–6583.
76. Daum, R. S.; Majumdar, S.; Bates, D. W.; Motta, A. T.; Koss, D. A.; Billone, M. C. On the embrittlement of Zircaloy-4 under RIA-relevant conditions. In *Zirconium in the Nuclear Industry: 13th International Symposium*. ASTM STP 1423, 2002; pp 702–718.